Coupled aeroelastic analysis of a free flight rocket

D.S. Livshits, S. Yaniv
IMI - Israel Military Industries
P.O.B. 47100 Ramat Hasharon, Israel

and

M. Karpel
Technion - Israel Institute of Technology
Haifa 32000, Israel

Abstract

Aeroelastic analysis of rockets is an essential part of their design procedure. In most cases, the analysis is limited to calculation of the divergence velocity, sometimes leading to unrealistic prediction of the rocket response. The coupled dynamic aeroelastic analysis approach is established to allow for the consideration of coupling effects between the rocket spin, its imperfection parameters and the airflow. The approach is based on integrated dynamic aeroelastic/CFD modeling methodology.

Introduction

Aeroelastic evaluation is one of procedures commonly used in rocket and missile design. Usually, such evaluation is limited to the calculation of the divergence velocity whose physical meaning can be explained as follows. Rocket flight can be divided into two phases: the powered phase and the free flight phase. During the powered phase the rocket accelerates from zero to the maximum velocity, also called the burnout velocity. During this phase of flight the rocket center of mass moves forward as a result of the propellant consumption. The aerodynamic center of the rocket also moves as a result of the variation of the rocket aerodynamic coefficients as a function of the flight velocity. The aerodynamic lift on the rocket body, especially on the nose and the tail, contributes to the rocket bending deformation, causing additional shift forward of the rocket aerodynamic center. This situation is shown schematically in Figure 1. The thin solid line in the figure indicates the movement of the rocket center of mass as a function of the rocket velocity. The dashed line shows the typical movement of the rigid rocket aerodynamic center. The thick solid line indicates the movement of the aerodynamic center of the flexible rocket. At certain velocity, called the divergence velocity, the shifted location of the aerodynamic center coincides with the location of the center of mass. When that happens, the rocket becomes unstable. Such condition is not permissible and, therefore, the burnout velocity is always kept below this divergence velocity. The ratio between the divergence velocity and the burnout velocity is called the divergence safety factor.

There are several commonly used methods to calculate the divergence velocity and the divergence safety factor, see Refs. [1] - [4]. Divergence analysis procedures outlined in these references assume that the rocket has no imperfections, no additional inertia forces caused by the rocket spin and that the rocket flies at constant velocity. The last assumption requires application of an iterative solution in order to calculate the actual divergence speed. In the present article, we are looking for a more accurate method that accounts for the spin and imperfection effects and allows obtaining a cut-off velocity above which the rocket might fail. The term “cut-off velocity” will be used throughout the article in order to emphasize the difference between the present method and the divergence analysis method. We define the cut-off velocity as a flight velocity for which the angle of attack and the loads associated with it exceed a certain limiting value. This limiting value is derived form the strength limit of the most sensitive rocket parts, usually, the rocket fins. In most cases the limiting value of the angle of attack for the burnout velocities of M=3.5-5.0 is about 0.5 degree. The cut-off velocity is always smaller than the divergence velocity. Keeping this in mind, one can consider the present analysis as a refinement of the divergence analysis.

Two imperfection parameters are used in the present research: the thrust misalignment and the dynamic imbalance. These imperfections are usually considered in the trajectory computations for the purpose of the accuracy evaluation. The primary coupling effect considered in the article, is the coupling between the airflow and the rocket bending deformation which is treated using MSC/NASTRAN Nonlinear Direct Transient Solution (SOL 129).

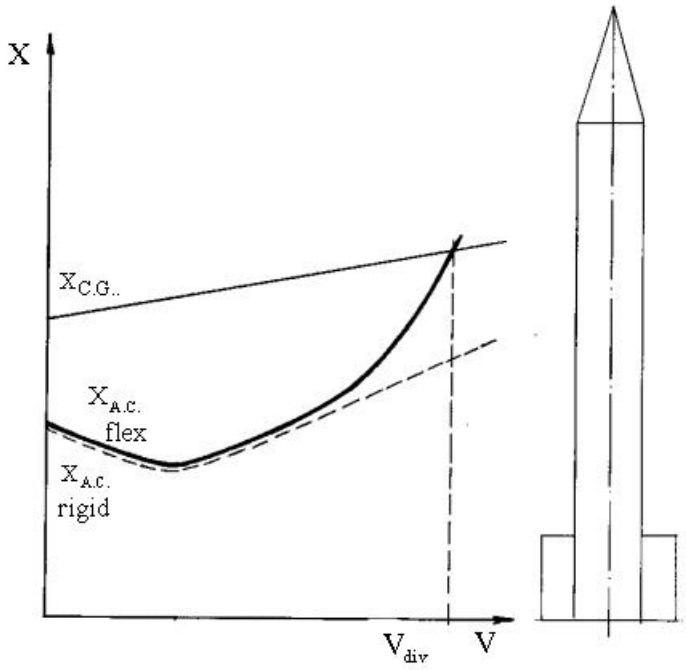

Figure 1. Typical movement of the center of gravity and the aerodynamic center as a function of the speed of flight.

Problem definition

The coupled dynamic aeroelastic response of the flexible rocket is computed using SOL 129 - Nonlinear Direct Transient solution of the MSC/NASTRAN version 68.2. The most general form of the rocket equations of motion is:

$$[M]\{\ddot{x}\}+[C]\{\dot{x}\}+[K]\{x\}=\left\{F\left(x,\dot{x},\dot{x}^2\right)\right\} \quad (1)$$

The mass matrix $[M]$ is the constant lumped mass matrix combined of BEAM and CONM2 elements. The stiffness matrix of the rocket $[K]$ is built using BEAM elements. The damping matrix $[C]$ is assumed to be proportional to $[K]$, so that $[C]=\alpha[K]$, where the parameter α is defined by the PARAM,W3 entry and PARAM,G. The external loads vector consists of the following parts:

1. Aerodynamic lift, defined for each structural element in the form:

$$L_i=\frac{1}{2}\rho_\infty AV^2 dC_{L_{\alpha i}}\alpha_i \quad (2)$$

where ρ_∞ is the air density in the far field, A is the reference area, V is the rocket velocity, d is the rocket diameter, α_i is the local angle of attack of the i-th element and $C_{L\alpha_i}$ is the local lift coefficient derivative.

This lift coefficient is derived from separate CFD computations, are based on the three dimensional Navier-Stokes equations for turbulent flow as described by Baldwin-Lomax turbulence model. After the appropriate nondimensionalization, the CFD equations are written in a Cartesian coordinate system (x,y,z) as:

$$\frac{\partial}{\partial t}\overline{W}+\frac{\partial}{\partial x}\overline{F}+\frac{\partial}{\partial y}\overline{G}+\frac{\partial}{\partial z}\overline{H}=0 \quad (3)$$

where

$$\overline{W} = \{\rho \quad \rho u \quad \rho v \quad \rho w \quad \rho E\}^T$$

$$\{\overline{F}, \overline{G}, \overline{H}\} = \{\overline{F}^i - \overline{F}^v, \overline{G}^i - \overline{G}^v, \overline{H}^i - \overline{H}^v\}$$

$\{\overline{F}^i, \overline{G}^i, \overline{H}^i\}$ is the inviscid flux vectors defined by:

$$\overline{F}^i = \{\rho u \quad \rho u^2 + p \quad \rho uv \quad \rho uw \quad \rho uH\}^T$$

$$\overline{G}^i = \{\rho v \quad \rho uv \quad \rho v^2 + p \quad \rho vw \quad \rho vH\}^T$$

$$\overline{H}^i = \{\rho w \quad \rho wu \quad \rho wv \quad \rho w^2 + p \quad \rho wH\}^T$$

and $\{\overline{F}^v, \overline{G}^v, \overline{H}^v\}$ is the viscous part of the flux vector, whose complete form is readily available in Ref. [5]. We use body-fitted computation grid defined by a multi-block algorithm that allows for local grid refinements. The numerical scheme is a finite volume scheme that uses centered differences and the explicit Runge-Kutta scheme in time. The rocket aerodynamic configuration is shown in Figure 2. Side and rear views on the CFD grid are shown in Figures 3 and 4, respectively. A typical pressure distribution around the configuration is shown in Figure 5. Since the CFD grid and the structural grid do not coincide, a simple procedure was developed to convert the pressure distribution around the rocket into local lift coefficient derivatives corresponding to the structural grid. These coefficients were computed for the Mach numbers M=0.0, 0.5, 1.0, 1.5, 2.0, 2.5, 3.0, 3.5, 4.0, 4.5, 5.0, and different angles of attack $\alpha = 0^o, 0.5^o, 1.0^o,$ assuming that the aerodynamic configuration is rigid. These computations and a linearization assumption allowed definition of the diagonal lift coefficient derivatives matrix $[C_{L\alpha}]$, introduced into the analysis model by means of the NOLIN1 entries, as described below. The same coefficients were used to compute the aerodynamic damping forces in the pitch mode:

$$L_i^D = \frac{1}{2}\rho_\infty AV^2 dC_{L\alpha_i} \frac{\theta \overline{x}_i}{V} = \frac{1}{2}\rho_\infty AV dC_{L\alpha_i} \theta \overline{x}_i \qquad (4)$$

where q is the pitch velocity of the rocket and $\overline{x}_i$ is the distance between the rocket center of mass and the i-th structural grid point.

Another part of the aerodynamic model is the aerodynamic drag which is defined by:

$$D_i = \frac{1}{2}\rho_\infty AV^2 C_D \frac{\ell_i}{\ell} \qquad (5)$$

where D_i is the drag force on the i-th grid point of the rocket model, C_D is the drag coefficient, a known function of the Mach number, ℓ is the rocket length and ℓ_i is the length of the i-th element. This forcing function is constructed by a combination of NOLIN1 and NOLIN2 entries.

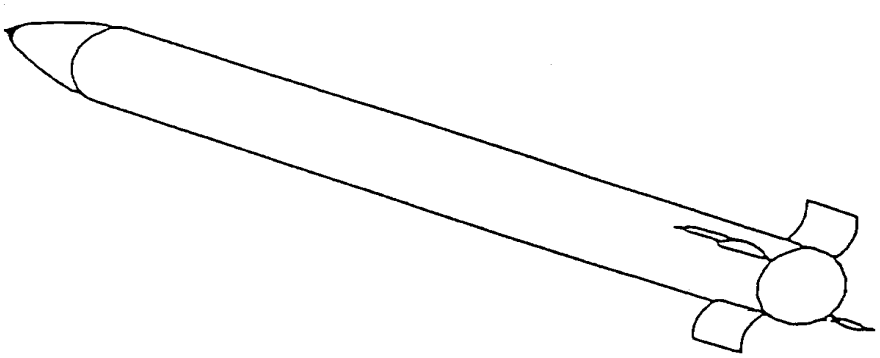

Figure 2. Generic rocket aerodynamic configuration

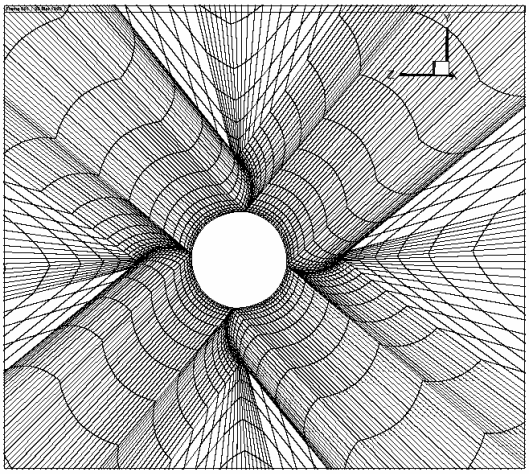

Figure 3 Rear view on the CFD grid.

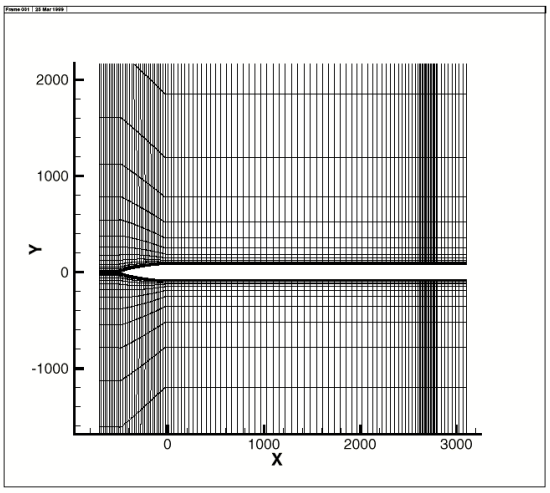

Figure 4 Side view on the CFD grid

2. Thrust T, defined as a follower force acting through a line connecting two structural points. The location of these grid points is the location of the rocket nozzle, allowing to account for the nozzle local stiffness. The thrust is a known function of time. Introduction of the thrust as a follower force requires the application of large displacement entry PARAM,LGDISP.

3. Distributed centrifugal forces acting as shown in Figure 5. These forces are also follower forces, defined by:

$$F_{C_i} = m_i \omega^2 \delta r_i \qquad (6)$$

where m_i is the mass associated with the i-th structural grid point; ω is the rocket spin, a known function of time; and δr_i is the radial distance between the spin axis and the distorted location of that grid point. The axis of rotation is assumed to run through the instantaneous location of the center of mass in the direction of the rocket instantaneous velocity. The instantaneous location of the center of mass is computed using the MPC entry and the following equation:

$$Z_{C.G.} = \frac{\sum_{i=1}^{N} m_i \delta z_i}{\sum_{i=1}^{N} m_i} \quad (7)$$

where δz_i is the distorted location of the i-th structural grid point. The radial distance δr_i is computed using the MSC/NASTRAN Transfer Functions and the following equation:

$$\delta r_i = \delta z_i - \theta_{C.G.} \bar{x}_i \quad (8)$$

where $\theta_{C.G.}$ is the pitch angle at the structural grid point closest to the rocket center of mass. The transfer functions are used in this case instead of the MPCs because the degrees of freedom connected by the MPCs are removed from the analysis set and cannot be used in NOLIN2 entries to compute the forcing function (6).

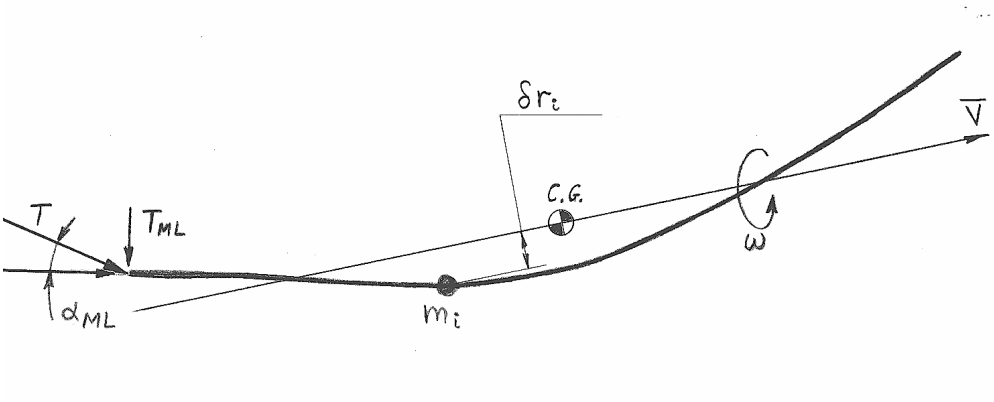

Figure 5 Centrifugal force and thrust application diagram

4. Thrust misalignment force. In the present research, the thrust misalignment is limited to the angular misalignment only, being applied per Figure 5 and equation:

$$T_{ML} = T\alpha_{ML} \quad (9)$$

where $\alpha_{ML} = 0.0001\,\text{rad}$ is the thrust misalignment angle. Another NOLIN2 entry is used to apply this force.

5. Dynamic imbalance. The dynamic imbalance means that the principal inertia axis of the rocket does not coincide with the geometry axis, and the angle between them is defined by:

$$\tan 2\alpha_{IB} = \frac{2I_{xy}}{I_{yy} - I_{xx}} \quad (10)$$

where I_{yy} and I_{xx} are the pitch/yaw and the roll moments of inertia respectively and I_{xy} is the cross product of inertia defined by:

$$I_{xy} = m_{IB}\frac{d}{2}\bar{x}_{IB} \tag{11}$$

where m_{IB} is the imbalance mass and $\bar{x}_{IB}$ is the distance between this mass and the rocket center of mass. The dynamic imbalance is simulated by:

$$F_{IB} = m_{IB}\omega^2\frac{d}{2} \tag{12}$$

Finite element model

The finite element model consists of three parts: the BEAM and CONM2 model of the rocket itself, the aerodynamic coefficients model created by dummy ROD elements and NOLIN1 entries, and the auxiliary model built of dummy RODs with MPCs, NOLINs and Transfer Functions. The entire model is shown in Figure 6. The dummy RODS are elements whose stiffness equals to unity and whose fundamental frequency is very high relative to the fundamental frequency of the rocket. The dummy RODs are used in order to generate the nonlinear forcing functions in a manner similar to the one described in Ref. [6]. Figure 7 contains the flowchart that was used to generate the centrifugal forcing function. This forcing function was not used in Ref. [6].

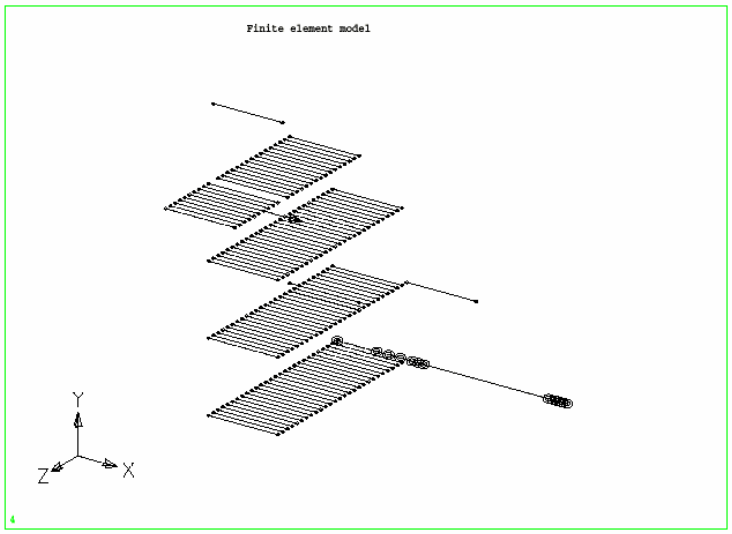

Figure 6 Entire finite element model.

Notes

1. The gravity force is not applied in this analysis, because we are not interested in computing the rocket trajectory, but the dynamic aeroelastic response only. The gravity force does not change the dynamic response.
2. The problem is solved as a planar one, meaning that the solution is obtained in a body fixed coordinate system where the aerodynamic lift forces are considered normal forces.
3. Centrifugal forces could not be applied using the RFORCE entry in SOL 129.

4. The rocket mass matrix remains constant throughout the entire solution, due to the MSC/NASTRAN limitations in SOL 129. These limitations provide slightly unconservative prediction of the rocket dynamic response in the first half of the powered phase of flight. Fortunately, rockets are usually very stable in this phase, as one can see in Figure 1, and some additional stability does distort the results significantly. However, for the future, it is desirable to include the option of variable mass in SOL 129.
5. Stabilizing gyroscopic effects of the rocket spin were neglected because the spin is not high enough. Usually, it becomes significant above 100 cps, whereas in our case it is kept below 25 cps.

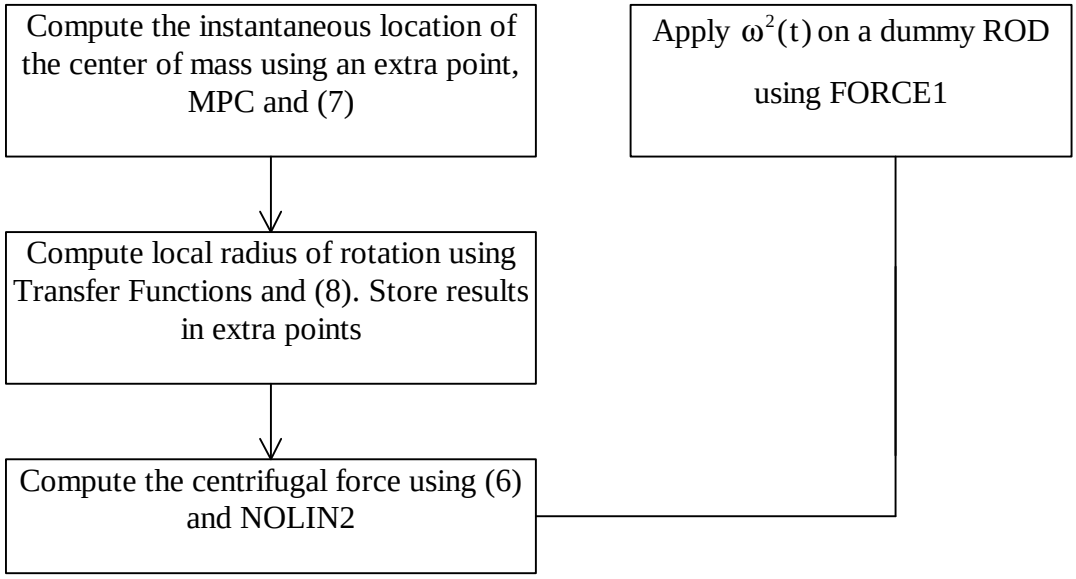

Figure 7 Flowchart to generate centrifugal forces in SOL 129

Finite element analysis

Several rockets were analyzed in the present investigation. The first one has steel motor case and steel warhead. Its dynamic response is presented in Figure 8. The Figure shows the time history of the angle of attack of the nose tip and the tail. The upper curve corresponds to the nose tip, and the lower curve corresponds to the tail. The vibration frequency in the figure is related to the short period frequency of vibration a typical frequency for a rigid body accelerating in the air stream. The vibration is initiated by the presence of an imperfection. The overall behavior of the dynamic response belongs to a stable rocket undergoing a usual type of response. Figure 9 shows the response of a rocket identical to the first one with only two modifications: the motor casing is replaced by a composite and the warhead is made of aluminum. From this figure we observe that after the burnout, the rocket behavior is governed by the spin, coupled with the bending deformation of the rocket. Such kind of behavior is usually undesirable even though the angle of attack does not exceed the cut-off value. The third rocket, whose dynamic response is shown in Figure 10 is identical to the second one, but its stiffness was reduced by a factor of 1.7. Such reduction can be a result of a flexible fitting between the motor casing and the warhead, etc. In this case, the rocket undergoes a divergent type of response and,

according to the simulation, is expected to fail in the flight test. Such result could not be predicted without incorporating the coupling effects in the simulations. As evident, Figure 11 shows the dynamic response of the last rocket with disabled spin effect. This response is similar to the one shown in Figure 8. Looking at this response one could erroneously conclude that the rocket would not fail.

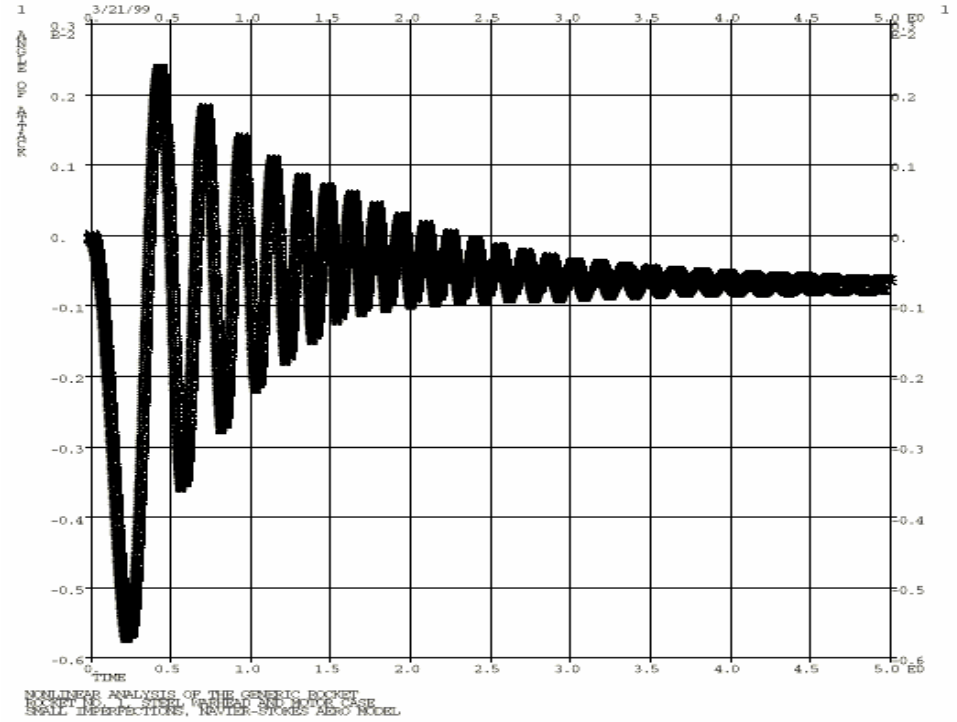

Figure 8 Dynamic response of a generic rocket with steel warhead and steel motor case

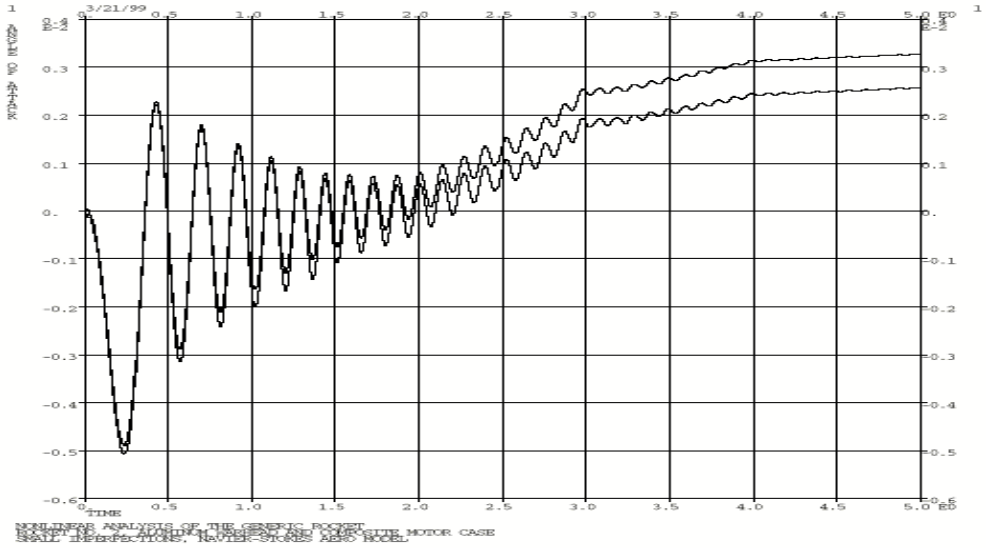

Figure 9 Dynamic response of the generic rocket with aluminum warhead and composite motor case

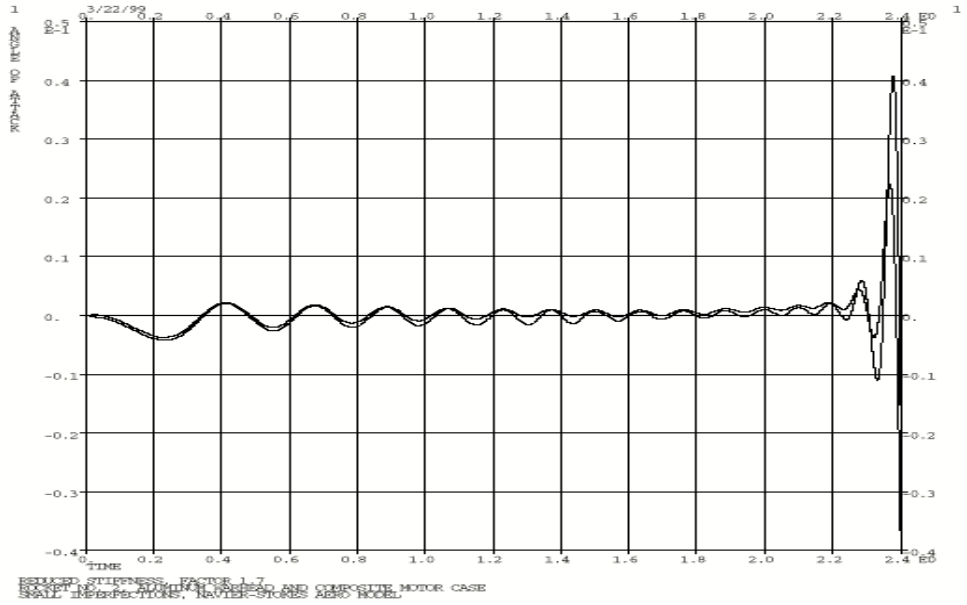

Figure 10 Dynamic response of the generic rocket with aluminum warhead, composite motor case and reduced stiffness.

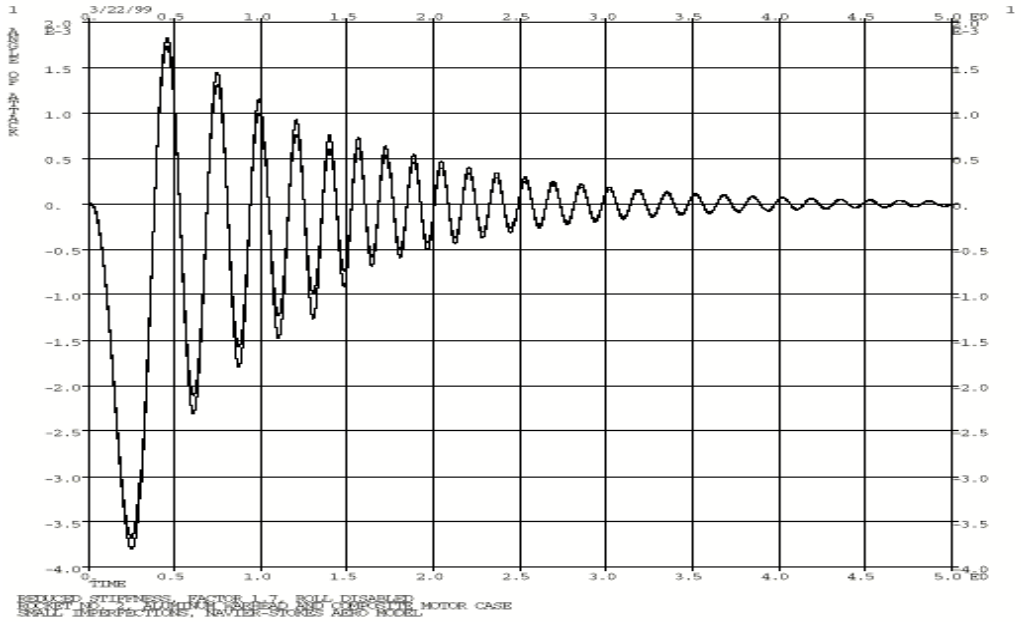

Figure 11 Dynamic response of the generic rocket with aluminum warhead, composite motor case and reduced stiffness with disabled spin.

Conclusions

1. Nonlinear coupled aeroelastic response can be calculated using the MSC/NASTRAN code, SOL 129 with certain limitations, like disregarding the effect of variable mass.
2. Coupling effects become very significant when rockets become more flexible. This flexibility can be a result of higher aspect ratio, utilization of lighter and stronger materials, improper design of fittings, etc. These effects can lead to a complete failure of the rocket, which might be overlooked without considering the cpupling effects.
3. From the results of the present investigation we can conclude that the aeroelastic simulation tool including the coupling effects is the only reliable one and therefore, must be an essential part of the design process.

References

1. Dov Elyada, "Closed-Form Approach to Rocket Vehicle Aeroelastic Divergence", *Journal of Spacecraft,* vol. 26, no. 2, pp. 95-102
2. O'Keepe D. A., "General Static Aeroelastic Analysis of a Body of Revolution", *AIAA Journal,* December 1965.
3. Glasson A. R. and Pearson R. G., " A FORTRAN Computer Program for Steady State Aeroelastic Evaluation of Slender Nonrolling Rocket Vehicles", Australian Defence Scientific Service, TN-HAS 128, October 1967.
4. Young C. P., "On the Steady State Aeroelastic Behavior of a Spinning Rocket Having Aerodynamic Asymmetry", AIAA Second Sounding Rocket Conference, Williamsburg, Virginia, 1970.
5. Hoffmann K. A., Chiang S. T., Siddiqui S., Papadakis M., *Fundamental equations of fluid mechanics,* Engineering Education Systems, 1996.
6. Livshits D. S., Saltoun D., "Nonlinear Analysis of Free Flight Rockets Using MSC/NASTRAN", 1995 MSC/NASTRAN World User's Conference, Florida.